ADVANCED MATERIALS
www.advmat.de

An Insight into the Phase Transformation of WS_2 upon Fluorination

Sruthi Radhakrishnan, Deya Das, Liangzi Deng, Parambath M. Sudeep, Guillaume Colas, Carlos A. de los Reyes, Sadegh Yazdi, Ching Wu Chu, Angel A. Martí, Chandra Sekhar Tiwary, Tobin Filleter,* Abhishek K. Singh,* and Pulickel M. Ajayan**

The transformation from semiconducting to metallic phase, accompanied by a structural transition in 2D transition metal dichalcogenides has attracted the attention of the researchers worldwide. The unconventional structural transformation of fluorinated WS_2 (FWS_2) into the 1T phase is described. The energy difference between the two phases debugs this transition, as fluorination enhances the stability of 1T FWS_2 and makes it energetically favorable at higher F concentration. Investigation of the electronic and optical nature of FWS_2 is supplemented by possible band structures and bandgap calculations. Magnetic centers in the 1T phase appear in FWS_2 possibly due to the introduction of defect sites. A direct consequence of the phase transition and associated increase in interlayer spacing is a change in friction behavior. Friction force microscopy is used to determine this effect of functionalization accompanied phase transformation.

The unique properties found in graphene and later in monolayers of other materials thrust the research on transition metal dichalcogenides (TMDs) as evidenced from the publications on TMDs in the past decade.[1–5] A distinctive property of TMDs is their polymorphic structural and electronic characteristics. For instance, in group 6 chalcogenides such as MoS_2 and WS_2, when the sulfur (S) atoms occur on top of each other, it results in trigonal prismatic symmetry in the commonly called 2H semiconducting phase and the displaced S atoms results in octahedral symmetry in the 1T metallic phase.[6] Li or K functionalization reduces the TMDs and the gliding of the S planes results in the transformation from 2H to 1T. Functionalization by other electron donating species such as Re, Tc, and Mn can also induce the transformation.[7–11] The electron donated by the alkali metals alters the d electron count of the metal (Mo or W), and it splits in the octahedral coordination to have three unpaired electrons in the valence band d orbitals. However, the 1T phase is highly unstable and converts back into 2H phase with time and temperature.[12]

Apart from alkali metals, several attempts have been made on the covalent functionalization of 2H and 1T phases by organic functional groups.[13–16] Sarkar et al. decorated the 2D layers with metal nanoparticles which changed the transfer characteristics of the 2D devices and demonstrated its capability as a gas sensor.[17] Theoretically, hydrogenation also converts the 2H semiconducting phase into the metallic phase.[18] A transformation from an n-type to a p-type semiconductor, a nonmagnetic to a magnetic material and a boost in the catalytic activity was achieved through controlled and selective doping of TMDs by transition metals.[19] An interesting deviation from extrinsic doping was intrinsic doping by the incorporation of islands of 1T in a lattice of 2H semiconducting nanosheets, where the

Dr. S. Radhakrishnan, Dr. C. S. Tiwary, Prof. P. M. Ajayan
Department of Materials Science and NanoEngineering
Rice University
Houston, TX 77005, USA
E-mail: cst.iisc@gmail.com; ajayan@rice.edu
Dr. D. Das, Prof. A. K. Singh
Materials Research Center
Indian Institute of Science
Bangalore 560012, India
E-mail: abhishek@mrc.iisc.ernet.in
Dr. L. Z. Deng, Prof. C. W. Chu
Texas Center for Superconductivity and Department of Physics
University of Houston
Houston, TX 77004, USA
Dr. P. M. Sudeep, Dr. G. Colas, Prof. T. Filleter
Department of Mechanical and Industrial Engineering
University of Toronto
Toronto, ON M5S3G8, Canada
E-mail: filleter@mie.utoronto.ca
C. A. de los Reyes, Prof. A. A. Martí
Department of Chemistry
Rice University
Houston, TX 77005, USA
Dr. S. Yazdi
Renewable and Sustainable Energy Institute
University of Colorado
Boulder, CO 80309, USA
Prof. C. W. Chu
Lawrence Berkeley National Lab
Berkeley, CA 94720, USA
Dr. C. S. Tiwary
Metallurgical and Materials Engineering
Indian Institute of Technology Kharagpur
West Bengal 721302, India

DOI: 10.1002/adma.201803366

exchange interaction between vacancies in the 1T islands gives rise to magnetism.[20]

Besides electronic structure and magnetism in TMDs,[21,22] their performance in energy storage, electrocatalysis, and lubrication are also influenced by the phase transformation.[23] Although the effect of phase transformation on lubrication could surpass the others, owing to the relevance of interlayer interaction in defining a materials lubricity, it is still a naive area.[24] The complexity of the known methods of 2H to 1T transformation, their instability, and undesired impurities might be contributing factors to the scarcity in literature examples.

In this article, we report the functionalization of 2H WS_2 with fluorine using a recently developed method.[25] Notably, a transformation from 2H to 1T phase is observed on fluorination, which is otherwise a result of functionalization by an electron donating species only. The transformation is verified by various techniques and clearly observed in annular dark-field scanning transmission electron microscopy (ADF-STEM) images. Through the calculation of formation energy, the stability of fluorinated tungsten disulfide (FWS_2) in the 1T and 2H phase is evaluated. The conversion of phase leads to transformation of electronic, optical, magnetic properties, and the interlayer interaction; which are reviewed in this paper experimentally and theoretically by density functional theory (DFT) calculations. A study of friction of WS_2 and FWS_2 reveals the effect of functionalization and phase transformation on possible applications of the materials.

Primarily, bulk WS_2 powder was exfoliated in *N,N*-dimethylformamide (DMF) by ultrasonication. The exfoliated sheets of WS_2 were used for subsequent fluorination in a hydrothermal reactor at 200 °C for 24 h.[25] Nafion, a fluoropolymer which degrades at 200 °C to give fluorine free radicals was used as the source of fluorine. The amount of precursor was varied to obtain various concentrations of fluorine. FWS_2 obtained after the reaction was thoroughly washed with acetone and dried. On comparison of the X-ray diffraction pattern (**Figure 1**a) of exfoliated WS_2 and FWS_2; the FWS_2 shows the appearance of the (001) plane peak, though the (002) reflection continues to be the most intense peak. The (001) peak in exfoliated WS_2 has previously been observed in the case of alkali metal intercalation which results in the conversion of the 2H semiconducting phase into the 1T metallic phase.[26] The calculation of the lattice constants show an increase in the value of "*a*" due to the strain induced by intercalation of fluorine. The appearance of fluorine peaks in X-ray photoelectron spectrum (XPS) further confirms the doping.

A detailed analysis of the photoelectron spectrum of W and S indicates the absence of any W–F or S–F bonding interaction. Elemental fluorine has a larger atomic size than lithium; however, it is much smaller than the interlayer spacing of WS_2 (0.6 nm). Hence, it would be reasonable to conclude that fluorine intercalates in the layered WS_2.[27] XPS is also an important tool in determining the phase changes in TMDCs. The metallic nature of 1T phase downshifts the binding energy, which can be observed in Figure 1b which plots the binding energy of W and S against the variation of fluorine concentration. Deconvoluted spectra are given in Figure S3 in the Supporting Information. Fluorine being a highly electronegative element is expected to cause a change in the electron density of the neighboring atoms resulting in an upshift in the spectral positions. The observed downshift hence indicates the conversion to the 1T phase as well as the lack of interaction of fluorine with W and S at low percentages. As the doping of fluorine further increases beyond 20%, fluorine interacts with WS_2 and consequently, the peaks shift to higher binding energies, although it is still lower than that found in pristine WS_2.

The different phases are also readily evident in the Raman spectrum. The lower modes are highly active in FWS_2, as indicated by the Raman maps and the Raman spectra in Figure 1c,d and Figure S2 in the Supporting Information. The pristine WS_2 belonging to the 2H phase predominantly displays the $E_{2g}(\Gamma)$ and $A_{1g}(\Gamma)$ modes from the in-plane and out of plane vibrations respectively.[28,29] On fluorination, these modes remain relatively unchanged although many lower order peaks seem to appear. The lower modes are otherwise inactive due to wave vector conservation rules.[30] The formation of the superlattice structure in 1T phase allows zone folding activating the zone edge modes at the M point. The peaks at J_1 (128 cm^{-1}), J_2 (173 cm^{-1}), and J_3 (292 cm^{-1}) are assigned to these lower order modes and the peak at 260 cm^{-1} is assigned to E_g mode. The appearance of E_g mode has also been previously associated with the presence of octahedrally coordinated MoS_2.[28] Strong second order peaks of $2E_{2g}$ (702 cm^{-1}) along with combination of the first order peaks were observed in FWS_2 (Figure S1a, Supporting Information). The origin of the peak is not ascribed to 4LA(M) mode, as it does not correspond to the frequencies observed in this case.[31] A second order process involves an excited electronic state, along with two phonons having opposite wave vectors.[32] In other words, the excitation laser energy should be able to cause an excitonic transition, and the calculations of energies agree with the assignment. The stability of the formed 1T state is verified by heating the FWS_2 in air for an hour and collecting the Raman spectra. The sample was stable, and no derogatory effect was found until 400 °C (Figure S1b, Supporting Information), while Li intercalated WS_2 is known to transform to more stable 2H phase at temperatures above 300 °C.[23] These observations raise the question about the transformation to 1T phase on doping with a highly electronegative element such as fluorine. According to foregoing reports, the transformation from 2H to 1T phase is induced by the atomic sliding of S plane, on intercalation and reduction of alkali metals such as lithium and potassium or transition metals such as rhenium.[8] On reduction, they donate an electron transforming the 2H phase into the more stable 1T phase.

Atomic resolution ADF-STEM imaging unambiguously revealed the transformation regions, from 2H to 1T phase, in the fluorinated WS_2 sample. The ADF-STEM image in Figure 1e shows the trigonal prismatic 2H phase of WS_2 sample before the fluorination process. The ADF-STEM signal is approximately proportional to the atomic number square (Z^2); therefore the bright and dark spots in this image are corresponding to W atoms and S atomic columns (composed of two S atoms), respectively. Figure 1f demonstrates the coexistence of 1T and 2H phases in the FWS_2 sample. The trigonal prismatic 2H phase on the top left of the image transforms into the octahedral 1T phase on the bottom right of the ADF-STEM image. Another ADF-STEM image that has captured such a phase transformation in a larger area and an electron energy loss spectrum (EELS) showing the presence of fluorine in the same region are shown in Figure S4 in the Supporting Information.

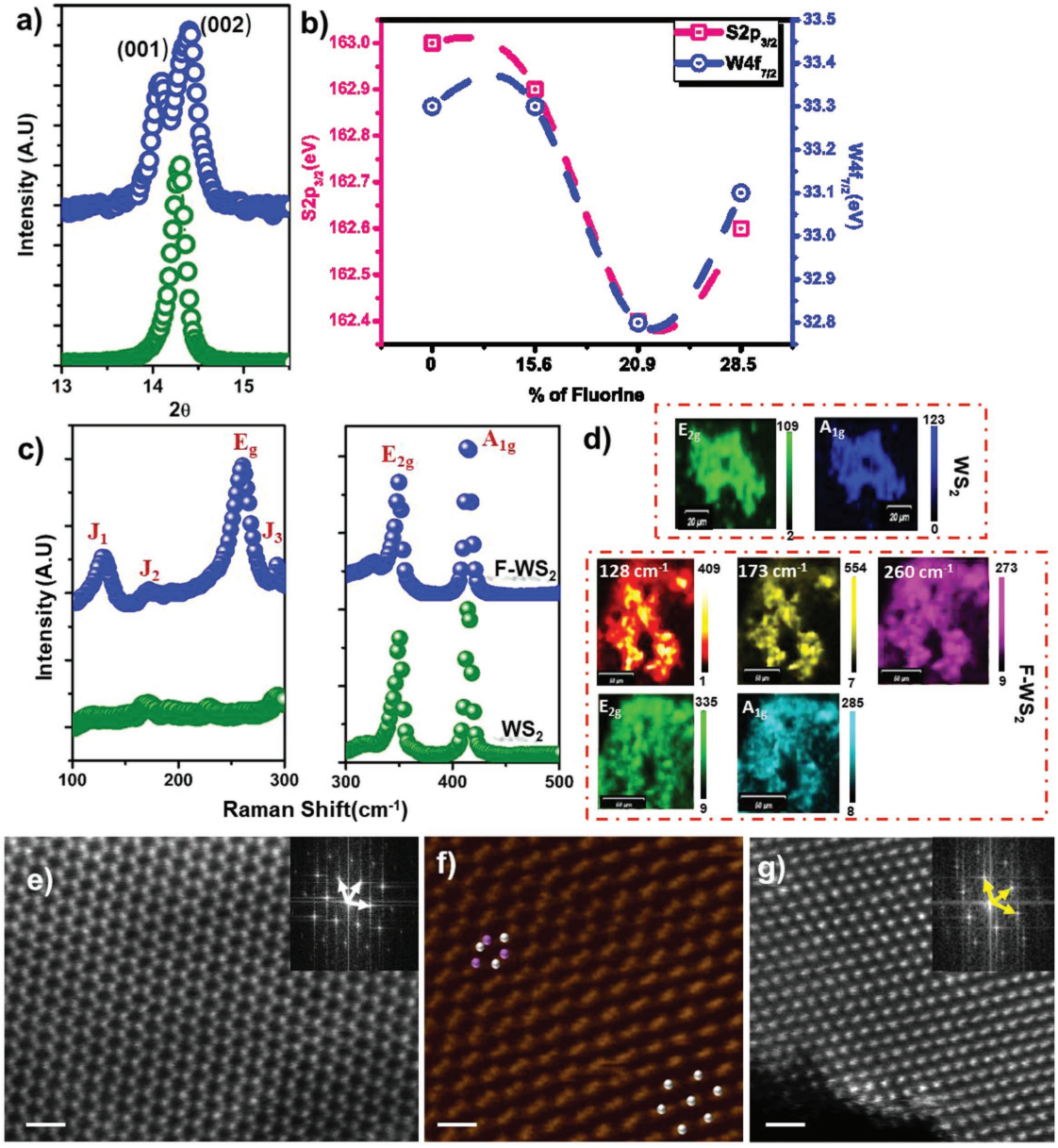

Figure 1. a) X-ray diffraction (XRD) spectrum of WS_2 (green) and FWS_2 (blue). b) The change in binding energy of $S2p_{3/2}$ and $W4f_{7/2}$ in X-ray photoelectron spectra with varying fluorine content measured at four different fluorine concentrations, the line joining the points show the general trend. c) Raman spectra of WS_2 and FWS_2. d) Raman maps of the two clearly showing the active lower modes (WS_2: Scale 20 µm; FWS_2: Scale 50 µm). e) Atomic resolution ADF-STEM image of WS_2 before fluorination. f) FWS_2 in which the purple colored spheres represent S atoms and silver spheres represent W atoms show the region of transformation. g) A region, completely transformed into 1T phase, with its corresponding fast Fourier transform (FFT) pattern shown in the inset.

WS_2 has been completely transformed to 1T phase in the area shown in Figure 1g in the FWS_2 sample.

First-principles-based theoretical calculations have been performed to understand the effect of fluorination on the phase transformation of WS_2. The structural and calculation details are given in Figure S12 in the Supporting Information. The semiconducting 2H WS_2 phase is more stable (0.89 eV per formula unit lower in energy) compared to metallic 1T phase, which is in well agreement with previous theoretical studies.[33] However, upon fluorination, the total energy difference between fluorinated 2H and 1T WS_2 reduces to 0.62 eV per formula unit, after adsorbing one fluorine atom in 4×4 WS_2 supercell (corresponding to 2.08% F concentration). The energy difference reduces as a function of F concentration as mentioned in Figure S12c in the Supporting Information, indicating that fluorination enhances the stability of 1T WS_2. At 66.66% F concentration, 1T FWS2 becomes energetically favorable compared to 2H FWS_2, clearly indicating 2H to 1T phase transformation. Additionally, we found that the formation energy of fluorinated 1T-WS_2 (with respect to bulk 1T WS_2) is 4.32 eV lower compared to fluorinated 2H-WS_2 (with respect to bulk 2H WS_2) for 2.08% F concentration. Therefore, 1T WS_2 phase

can be fluorinated easily compared to 2H WS_2 phase. This indirectly supports our experimental observation of 2H to 1T WS_2 phase transition upon fluorination. The formation energies of both fluorinated 2H and 1T WS_2 have been plotted as a function of F concentration up to 33.33% as shown in Figure S12d in the Supporting Information. As the number of adsorbed F atom increases, the trend remains the same, however, the formation energy difference between two phases decreases.

The total energy difference and formation energy calculations shed light only on thermodynamic stability. However, in experimental environments under higher temperatures, the kinetics involved in fluorinated WS_2 would also control the phase transformation and it is difficult to capture via theoretical calculations. Therefore, theoretically obtained value of fluorine concentration which leads to the phase transformation is higher than experimental observation. Nevertheless, the trends observed from theoretical calculations explain the phase transformation.

The absorption spectra of WS_2 in **Figure 2**a show the optical signatures of A, B, and C excitons. A excitonic peak is caused by the direct optical transition from the highest spin-split valence band to the lowest conduction band. In FWS_2, the A excitonic peak shifts to lower energy due to the shift in valence band position caused by the heavy p-type doping of fluorine. In addition to the shifting peak position, with increasing fluorine doping the A excitonic peak becomes broader and splits into multiple peaks. This has been previously observed in MoS_2, on controlling the doping concentration with the application of gate voltage and attributed to the creation of trions an excited state of two electrons and a hole.[34,35] The large binding energy of these trions enable them to be observed even at room temperature.[34] The presence of trions is usually weighed on the excitonic peaks; as the trion peaks dominate the excitonic peaks weaken. Here we see an increase in the B and C excitonic peaks, which could be due to the inhomogeneity of the wet chemistry-based doping.

While the absorption spectra point to the alteration of the optical band structure, the resistance vs temperature (*R–T*) measurements of WS_2 and FWS_2 in Figure 2b and Figure S6 in the Supporting Information depict the alteration of the electronic band structure. Though the *R–T* curve does not show a complete transformation into a metallic behavior, marked difference can be seen in the behavior of the two samples. Oddly, the decrease in resistance of FWS_2 to about room temperature shows an increase in available carriers for excitation on doping with fluorine. Noticeably, the resistance temperature curve of WS_2 remains uninfluenced by magnetic field, while that of FWS_2

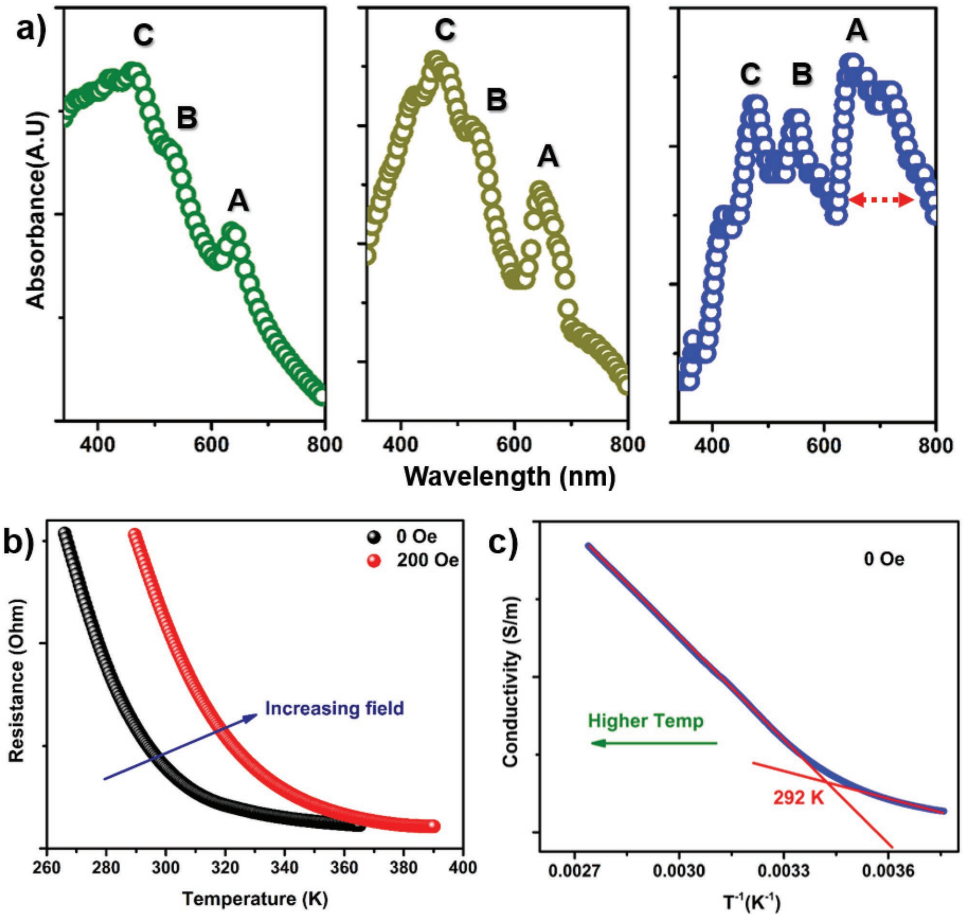

Figure 2. a) Absorption spectra of pure WS_2 (green) fluorinated WS_2 at two different fluorine concentrations (yellow and blue) showing the different excitonic transitions. b) The *R–T* curve of FWS_2 displaying a change with the applied field of 200 Oe and c) fitted conductivity versus temperature curve showing the change in hopping transport behavior.

changes with the application of magnetic field. The conductivity versus T^{-1} plot shows a change in scaling at a characteristic temperature, due to the change in hopping behavior with temperature as observed previously in the case of MoS_2.[36] The localization of charge carriers at the defects leads to this observed hopping behavior, and a reduction of the hopping probability with magnetic field is responsible for the change in R–T behavior on application of magnetic field.[37]

The change in electronic structure is further investigated by calculating spin-polarized band structures using first-principles calculations. 2H phase of WS_2 is semiconducting in nature having 1.78 eV of direct bandgap at the K point (shown in **Figure 3**a), which matches well with earlier reported values.[38] The unstable 1T phase is known to be metallic (shown in Figure 3b).[39] There are four bands which crosses each other at K point just above the Fermi level in 1T-WS_2 band structure. Upon fluorination in 1T WS_2 sheet, due to extra electrons from F atom, the empty bands get filled and go below the Fermi level as shown in Figure 3c–e. When one F atom is adsorbed, Bader charge analysis[40–42] shows that the F atom accumulates 0.53 electronic charge from S atoms of WS_2 sheet. The direct transition from valence band maxima (VBM) to conduction band minima (CBM) at K point originates the dominant A peak in the exciton spectra. The other two peaks (B and C) occur due

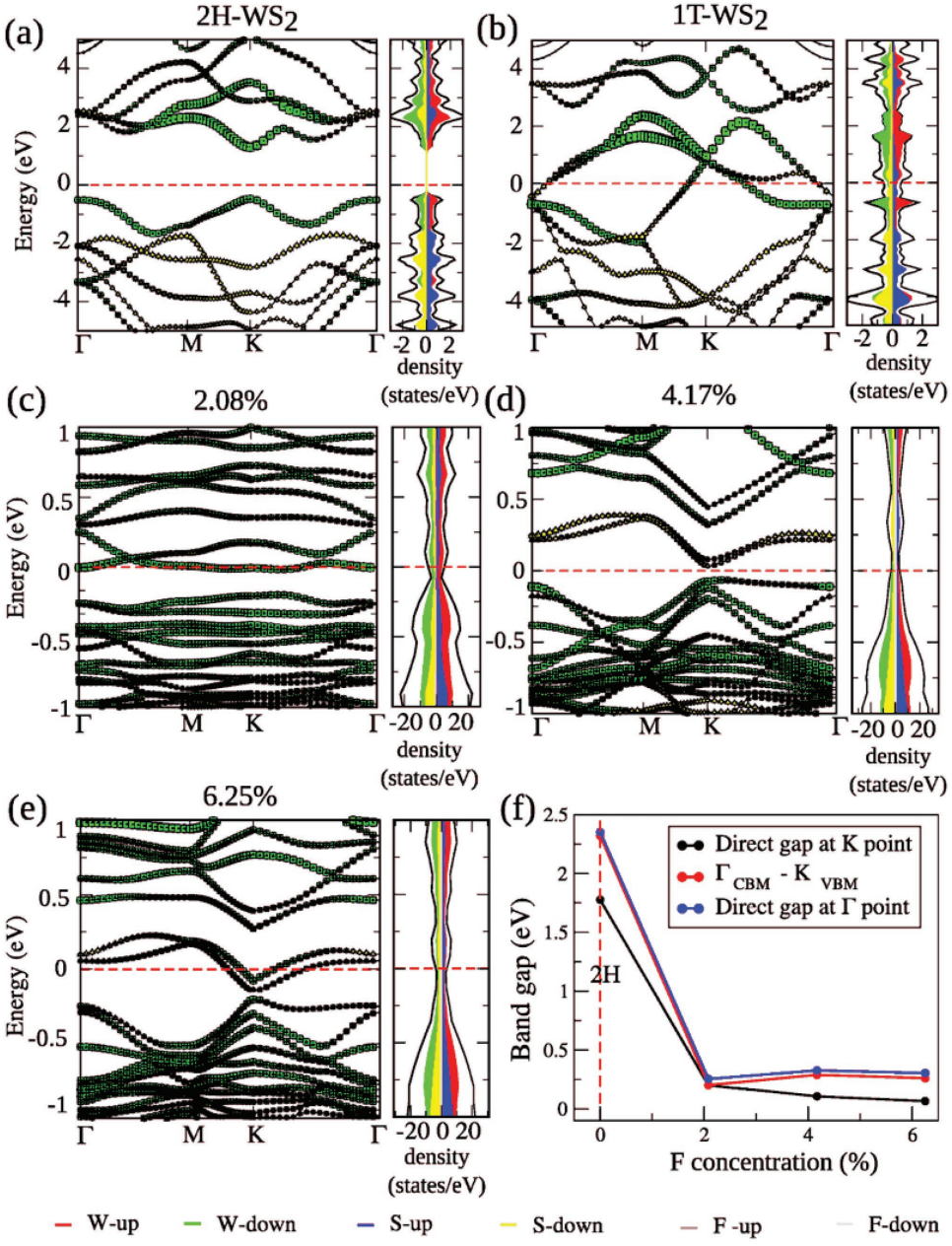

Figure 3. Band structures for: a) 2H-WS_2, b) 1T-WS_2 and fluorinated 1T-WS_2 having F concentrations of: c) 2.08%, d) 4.17%, and e) 6.25%. Band structures shown in (a) and (b) are calculated for one-unit cell whereas (c)–(e) are calculated for 4×4 unit cell. f) Change in direct bandgaps (separately at K and Γ point) and the indirect bandgaps (between VBM at K point and CBM at Γ point) as a function of F concentration.

to the direct transition from VBM to CBM at Γ point and the indirect transition from VBM at K point to CBM at Γ point, respectively. Three significant bandgaps which lead to three most dominant peaks in the exciton spectra are plotted as a function of F concentration in Figure 3f where at 0% F concentration, the bandgap of 2H WS_2 is shown. As F concentration increases, the direct bandgap between CBM and VBM at K point reduces for 1T FWS_2. Therefore, the reduction in direct bandgap at K point causes the shift of A peak in exciton spectra to longer wavelengths. The direct gap at Γ point and the indirect gap between VBM at K point to CBM at Γ point reduces overall for fluorinated 1T WS_2 as compared to 2H WS_2. However, these two bandgaps increase as a function of F concentration till 4.17% and remain almost same for 6.25% F concentration.

The spin paired electrons in the 2H semiconducting phase of WS_2 makes it a diamagnetic material at room temperature (**Figure 4**a). The low temperature (30 K) measurement of magnetic susceptibility displays a positive moment at low temperature, which is too weak that the diamagnetic background dominates. However, FWS_2 is ferromagnetic in nature (Figure 4b) due to the presence of unpaired d orbital electrons, owing to which phase incorporation of 1T in 2H is used to introduce magnetic centers in the nonmagnetic material. The room temperature hysteresis measurement of FWS_2 displays an overlap of ferromagnetic and paramagnetic nature, which is also revealed from the low temperature behavior. The temperature-dependent zero-field-cooled and field-cooled (ZFC–FC) curves almost overlap with a very small difference. This behavior verifies the overlap of paramagnetic and ferromagnetic ordering. A transition is also observed at temperature ≈52 K, as seen from the diverging ZFC–FC curves in Figure 4c,d. Reports on the calculation of the magnetism in MoS_2 has shown that the paramagnetic ordering comes from the change in coordination from trigonal to octahedral which creates two unpaired electrons in the d orbitals of the transition metal, while the redistribution of charges in WS_2 on introduction of fluorine could give rise to the ferromagnetism.[43] Ataca et al. investigated the origin of magnetism on doping with various elements as well as due to the introduction of vacancies, where he showed that a redistribution of charge densities around a triplet vacancy creates a moment of 2 μ_B.[44] While vacancies and unpaired electrons in the 1T phase can give rise to a significant magnetic moment, it has been shown that the spin exchange interactions between the transition metals is antiferromagnetic and hence the magnetism cannot be significant. Only those transition metal atoms in the radius of a vacancy can interact to align their spins to generate magnetic ordering.[45]

Theoretically using first-principles calculations, it has been reported that ferromagnetism can be induced in MoS_2 nanosheets by applying tensile strain and creating vacancies.[46] Cai et al. reported 2H to 1T local phase transformation in MoS_2 nanosheet by introducing S vacancies, which further leads to robust ferromagnetism.[45] In this work, magnetic properties have been studied by introducing S vacancy in 1T

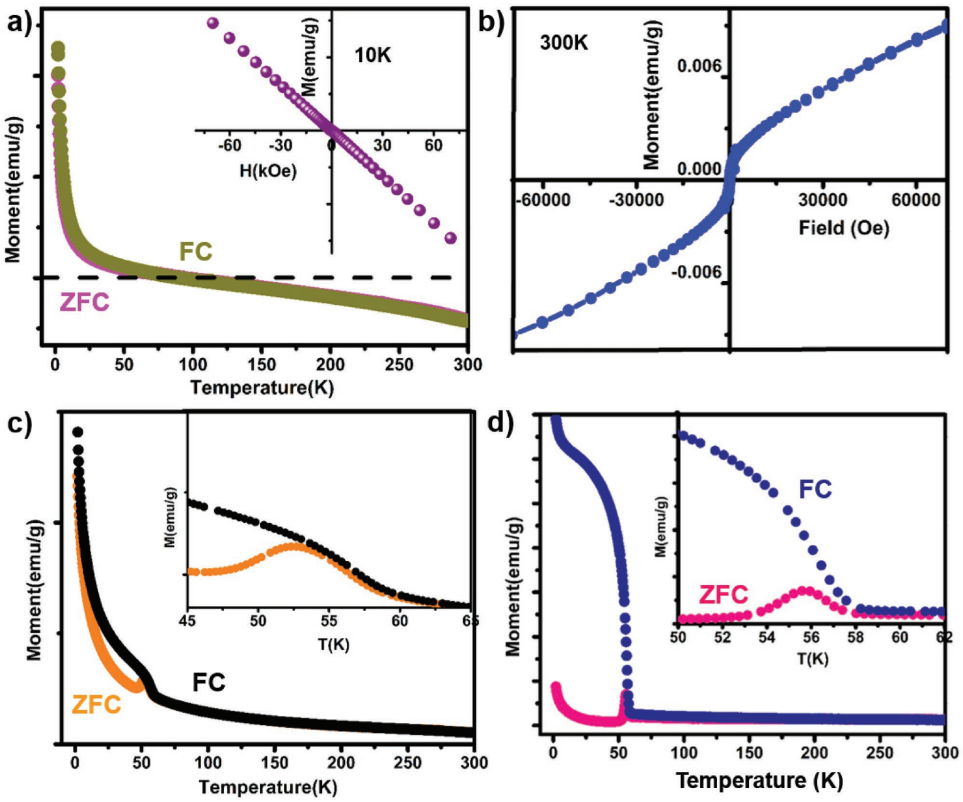

Figure 4. a) The ZFC–FC curve of pure WS_2 with the low temperature hysteresis curve on the inset. b) The room temperature hysteresis curve of FWS_2. c,d) ZFC–FC curves for FWS_2 at 5000 Oe (c) and 50 Oe (d).

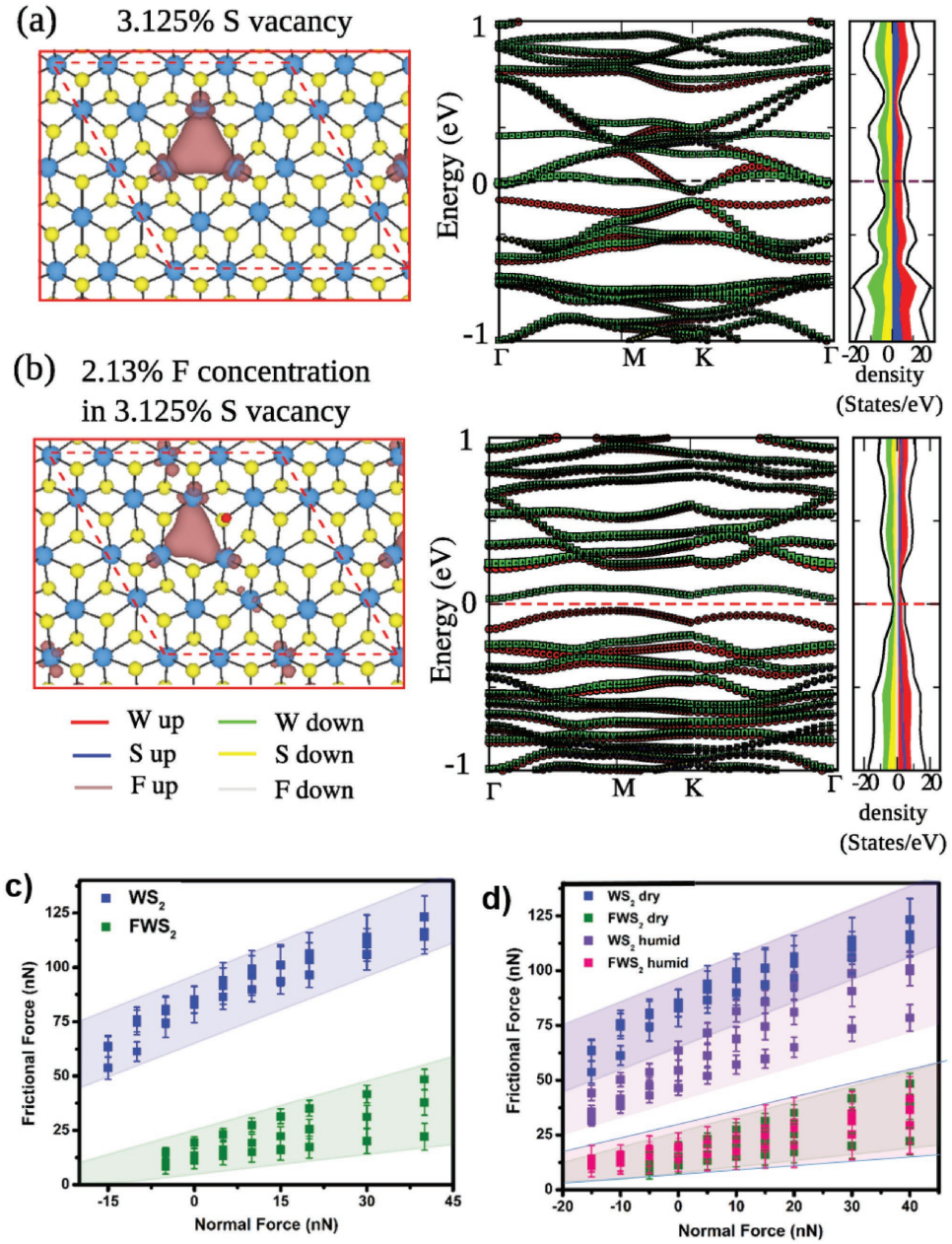

Figure 5. Spin-polarized band structure and density of states with structures for: a) 1T WS_2 with 3.125% S vacancy and b) 2.13% fluorinated 1T WS_2 with 3.125% S vacancy. The isosurface value of 0.002e A^{-3} is fixed for spin density (marked in brown color) plots. Frictional force versus normal load measured by frictional force microscopy of pristine and fluorinated WS_2 on a SiO_2/Si substrate in: c) dry conditions and d) dry and humid conditions overlapped (sliding speed: 5 μm s^{-1}).

WS_2 monolayer. Removal of one S atom from 4 × 4 1T WS_2 monolayer (3.125% S vacancy) exhibits ferromagnetism of 0.67 μ_B. In pristine WS_2, per formula unit, W atom donates two electrons total and each S atom gains one electron. After creating one S vacancy, there will be one unpaired electron which gets distributed in three neighboring W atoms contributing to ferromagnetism as shown in **Figure 5**a. The band structure and density of states confirm that the magnetization occurs due to the difference between up and down spin states of W atoms. After fluorination with 2.13% F concentration in this structure, W atoms close to S vacancy reduces electronic charge as F atom accumulates charge from both W and S atoms. However, charge transfer happens more from S atoms to F atom and magnetism retains due to the unpaired electrons of neighboring W atoms, exhibiting 0.7 μ_B of magnetization. The electron coming from F atom fills the empty bands which shift below the Fermi level as shown in Figure 5b. In addition to the induction to ferromagnetism, S vacancies found to enhance the stability of 1T phase of TMDs.[47] Transmission electron microscopy (TEM) images (Figure S2, Supporting Information) of our sample clearly show the presence of S vacancies, which might be the reason for its outstanding stability as well as ferromagnetism.

Having observed the chief evidences of phase transformation, we now evaluate its influence on friction of the materials. Of the many factors influencing the weak interlayer interaction and super lubricity in 2D materials, defects, atomic scale roughness, wrinkles, surface chemistry or surface passivation are primary. On fluorination of WS_2 several of these properties can be influenced/altered. In order to observe the effect of fluorination on the functionality of WS_2, we study the friction of 2D layered WS_2 and FWS_2 using frictional force microscopy.

The friction of FWS_2 is found to be lower than that of pristine WS_2 (Figure 5c,d) for both humidity conditions studied. This differs from the trend observed in previous friction measurements of fluorinated graphene which exhibit higher friction as compared to pristine graphene.[48,49] In the case of graphene, the presence of covalently bonded fluorine, which converts the sp^2 hybridized carbon into sp^3 hybridization, increases the surface corrugation, which could be one of the main contributors to the increased friction.[48] On the contrary, in the case of F-WS_2, XPS measurements as well theoretical simulations demonstrate a lack of covalent bonding between F and WS_2, instead the F atom intercalate between the layers of WS_2 which increases the interlayer spacing. This lack of surface bonding likely does not increase the corrugation of the interfacial potential, instead; the phase transformation accompanied by reduced interlayer interaction and presence of weakly bound F intercalation results in lowering the friction. The lower friction for FWS_2 may also be indicative of a reduced interfacial potential corrugation for the T1 phase as compared to the 2H phase of WS_2. Another factor that may contribute would be the electronegativity of fluorine. It was reported that F atom could reduce the electron density of W and S and increase the layer separation, which would weaken the van der Walls force between WS_2 layers and reduces the energy for inter layer sliding thereby reducing friction.[50] Interestingly FWS_2 exhibits no major changes in friction under humid and dry condition. The observed friction reduction compared to the pristine material appears consistent with the larger scale friction behavior of fluorinated carbon,[51] fluorinated single wall carbon nanotubes[52] and WS_2/CFx coatings.[53]

On the other hand, the pristine WS_2 is sensitive to humidity and exhibits lower friction at 40% relative humidity (RH) than that of at 10% RH. We believe that the discrepancy is likely due to the reduced hydrophilic nature of WS_2, as compared to FWS_2 (Figure S8, Supporting Information). In the nonwear regime of friction, excess water can act to lubricate the contact between hydrophobic surfaces because the hydrophobicity implies easy shear and greater mobility of the capillary formed water layer within the contact-confined volume. In the case of the more hydrophobic WS_2, a liquid-like water film may form within the contact under humid conditions similar to water films formed on partially hydrophobic SiO_2.[54] Future atomistic simulations are needed to fully understand the underlying friction mechanisms, such as the WS_2 phase transformation effect on the interfacial energy corrugation and the influence of adsorbed water molecules.

In this article we try to give a perspective on the fluorine induced transformation of 2H WS_2 to 1T and the consequent changes in the optical, magnetic, and tribological properties. The structural transformation is supported by the microscopy images and fundamental characterizations of diffraction and Raman spectroscopy. DFT calculations show that fluorination enhances the stability of 1T FWS_2 and makes it energetically more stable compared to 2H FWS_2 at higher F concentration. The optical transitions of fluorinated WS_2 preserve the excitonic transitions in 2H WS_2 while showing signatures of trions. These are caused by the doping of TMDs by various methods. The low temperature electrical measurements do not show a metallic characteristic though supports hopping transport as a result of the introduction of defects. Theoretically, a decrease in the bandgap is observed on introduction of fluorine, and defects are observed to create magnetic centers, with experimental evidence of a combination of paramagnetic and ferromagnetic centers. It is derived from the observations that fluorination causes localized structural transformation in the WS_2 to the 1T phase. However, a complete transformation is not observed, and it creates a number of defects which brings about the behavior of doped WS_2. To assess the impact of these changes in intrinsic properties on the functionality of WS_2, the friction of WS_2 and FWS_2 was measured at different humidities. The friction of FWS_2 is lower than WS_2 and remains unaffected by the level of humidity.

Experimental Section

High-resolution electron microscopy images and EELS were acquired using an aberration corrected FEI Titan Themis^3 STEM. Raman studies were performed on Reinshaw inVia Raman Microscope. UV–vis absorption measurements were performed on a Shimadzu 2450 UV-Visible Spectrophotometer in the range of 190–800 nm. A magnetic property measurement system (MPMS) by Quantum Design was used for magnetic measurements. A physical property measurement system (PPMS) by Quantum Design measured the temperature-dependent conductivity. For the measurement of friction, materials were drop-cast on a Si wafer (285 nm thick oxide top layer), friction was characterized with a Si tip with a native SiO_2 layer (≈50 nm in diameter, cantilever normal spring constant ≈3 N/m) using an MFP-3D atomic force microscope (Asylum Research). Contact conditions were determined to stay in the nonwear regime of friction, at both 40% and 10% RH and room temperature.

The synthesis methodology used for FWS_2 was previously reported for fluorinated boron nitride.[25] Nafion, a fluoropolymer was used as the precursor for fluorine. Nafion degrades at 200 °C to give fluorine-free radicals. For the synthesis of FWS_2, a maximum of 1000 µL of nafion was used. Excess of nafion is undesirable and leaves behind polymer residues. Hence the amount of nafion is kept to a minimum. The amount of solvent which in turn dictates the pressure was determined by several iterations at various concentrations. 30 mL of the exfoliated WS_2 in DMF was used for the synthesis.

Theoretical Methodology: Theoretical calculations were performed using DFT as implemented in Vienna ab initio simulation package. The electron–ion interactions and electronic exchange correlations are incorporated by using an all-electron projector augmented wave potential and the Perdew–Burke–Ernzerhof generalized gradient approximation, respectively. The Brillouin zone is sampled using well converged Monkhorst–Pack scheme. The spin charge density is plotted using the visualization software VESTA.

Supporting Information

Supporting Information is available from the Wiley Online Library or from the author.

Acknowledgements

D.D. and A.K.S. thank Dr. A. Samanta for useful discussions. CST acknowledges funding support from Ramanujan fellowship. S.R., C.S.T., and P.M.A. acknowledge support from the Air Force Office of Scientific Research (AFOSR) Grant No. BAA-AFOSR-2013-0001. A.A.M. acknowledges the National Science Foundation (grant CHE 1610175) for financial support. L.Z.D. and C.W.C. thank the US Air Force Office of Scientific Research Grant FA9550-15-1-0236, the T. L. L. Temple Foundation, the John J. and Rebecca Moores Endowment, and the State of Texas through the Texas Center for Superconductivity at the University of Houston for financial support. D.D. and A.K.S. acknowledge Department of Science and Technology Nano Mission for financial support and thank "SahasraT," Cray XC40 Cluster of Supercomputer Education and Research Center and Materials Research Center, Indian Institute of Science, Bangalore for providing the required computational facilities. T.F. acknowledges support from the Natural Sciences and Engineering Research Council (NSERC) of Canada, the Canada Foundation for Innovation, and the Erwin Edward Hart Professorship.

Conflict of Interest

The authors declare no conflict of interest.

Keywords

2D magnetism, DFT calculations, fluorination, phase transformation, TMDs

Received: May 27, 2018
Revised: August 20, 2018
Published online: September 21, 2018

[1] G. R. Bhimanapati, Z. Lin, V. Meunier, Y. Jung, J. Cha, S. Das, D. Xiao, Y. Son, M. S. Strano, V. R. Cooper, L. Liang, S. G. Louie, E. Ringe, W. Zhou, S. S. Kim, R. R. Naik, B. G. Sumpter, H. Terrones, F. Xia, Y. Wang, J. Zhu, D. Akinwande, N. Alem, J. A. Schuller, R. E. Schaak, M. Terrones, J. A. Robinson, *ACS Nano* **2015**, *9*, 11509.
[2] Y. Yifu, N. Gwang-Hyeon, H. Qiyuan, W. Xue-Jun, Z. Kang, Y. Zhenzhong, C. Junze, M. Qinglang, Z. Meiting, L. Zhengqing, R. Fei-Rong, W. Xingzhi, L. Hai, H. Xiao, L. Bing, X. Qihua, Z. Qing, L. Zheng, G. Lin, D. Yonghua, H. Wei, H. Zhang, *Nat. Chem.* **2018**, *10*, 638.
[3] Z. Xiao, L. Zhuangchai, M. Qinglang, H. Zhang, *Chem. Soc. Rev.* **2018**, *47*, 3301.
[4] T. Chaoliang, L. Zhimin, C. Apoorva, C. Yongqing, D. Yonghua, G. Yue, H. Ying, L. Zhuangchai, Z. Xiao, Z. Lirong, Q. Xiaoying, H. Min, W. Goh-Jie, H. Shikui, W. Xue-Jun, G. Lin, K. Christian, H. Zhang, *Adv. Mater.* **2018**, *30*, 1705509.
[5] L. Zhuangchai, C. Apoorva, W. Yun, T. Thu-Ha, L. Xiaozhi, T. Chaoliang, L. Zhimin, C. Bo, H. Ying, N. Gwang-Hyeon, Z. Zhicheng, C. Ye, H. Zhaoning, L. Bing, X. Shibo, Z. Qinghua, Z. Yun, G. Lin, K. Christian, D. Yonghua, H Zhang, *J. Am. Chem. Soc.* **2018**, *140*, 8563.
[6] R. Kappera, D. Voiry, S. E. Yalcin, B. Branch, G. Gupta, A. D. Mohite, M. Chhowalla, *Nat. Mater.* **2014**, *13*, 1128.
[7] A. N. Enyashin, L. Yadgarov, L. Houben, I. Popov, M. Weidenbach, R. Tenne, M. Bar-Sadan, G. Seifert, *J. Phys. Chem. C* **2011**, *115*, 24586.
[8] Y. C. Lin, D. O. Dumcenco, Y. S. Huang, K. Suenaga, *Nat. Nanotechnol.* **2014**, *9*, 391.
[9] S. Kim, S. Song, J. Park, H. S. Yu, S. Cho, D. Kim, J. Baik, D. H. Choe, K. J. Chang, Y. H. Lee, S. W. Kim, H. Yang, *Nano Lett.* **2017**, *17*, 3363.
[10] Y. Wang, J. Xiao, H. Zhu, Y. Li, Y. Alsaid, K. Y. Fong, Y. Zhou, S. Wang, W. Shi, Y. Wang, A. Zettl, E. J. Reed, X. Zhang, *Nature* **2017**, *550*, 487.
[11] Q. Zhang, Y. Xiao, T. Zhang, Z. Weng, M. Zeng, S. Yue, R. G. Mendes, L. Wang, S. Chen, M. H. Rümmeli, L. Peng, L. Fu, *Chem. Mater.* **2017**, *29*, 4641.
[12] J. S. Sandoval, D. Yang, R. F. Frindt, J. C. Irwin, *Phys. Rev. B: Condens. Matter* **1991**, *44*, 3955.
[13] X. Chen, A. R. McDonald, *Adv. Mater.* **2016**, *28*, 5738.
[14] J. I. Paredes, J. M. Munuera, S. Villar-Rodil, L. Guardia, M. Ayán-Varela, A. Pagán, S. D. Aznar-Cervantes, J. L. Cenis, A. Martínez-Alonso, J. M. D. Tascón, *ACS Appl. Mater. Interfaces* **2016**, *8*, 27974.
[15] Q. Tang, D. Jiang, *Chem. Mater.* **2015**, *27*, 3743.
[16] L. Sun, X. Yan, J. Zheng, H. Yu, Z. Lu, S. Gao, L. Liu, X. Pan, D. Wang, Z. Wang, P. Wang, L. Jiao, *Nano Lett.* **2018**, *18*, 3435.
[17] D. Sarkar, X. Xie, J. Kang, H. Zhang, W. Liu, J. Navarrete, M. Moskovits, K. Banerjee, *Nano Lett.* **2015**, *15*, 2852.
[18] Y. Qu, H. Pan, C. T. Kwok, *Sci. Rep.* **2016**, *6*, 34186.
[19] A. A. Tedstone, D. J. Lewis, P. Brien, *Chem. Mater.* **2016**, *28*, 1965.
[20] L. Cai, J. He, Q. Liu, T. Yao, L. Chen, W. Yan, F. Hu, Y. Jiang, Y. Zhao, T. Hu, Z. Sun, S. Wei, *J. Am. Chem. Soc.* **2015**, *137*, 2622.
[21] Z. Hu, Z. Wu, C. Han, J. He, Z. Ni, W. Chen, *Chem. Soc. Rev.* **2018**, *47*, 3100.
[22] M. Zeng, Y. Xiao, J. Liu, K. Yang, L. Fu, *Chem. Rev.* **2018**, *118*, 6236.
[23] M. Chhowalla, D. Voiry, J. Yang, H. S. Shin, K. P. Loh, *MRS Bull.* **2015**, *40*, 585.
[24] J. C. Spear, B. W. Ewers, J. D. Batteas, *Nano Today* **2015**, *10*, 301.
[25] S. Radhakrishnan, D. Das, A. Samanta, C. A. Reyes, L. Deng, L. B. Alemany, T. K. Weldeghiorghis, V. N. Khabashesku, V. Kochat, Z. Jin, P. M. Sudeep, A. A. Martí, C. Chu, A. Roy, C. S. Tiwary, A. K. Singh, P. M. Ajayan, *Sci. Adv.* **2017**, *3*, e1700842.
[26] M. Acerce, D. Voiry, M. Chhowalla, *Nat. Nanotechnol.* **2015**, *10*, 313.
[27] H. L. Tsai, J. Heising, J. L. Schindler, C. R. Kannewurf, M. G. Kanatzidis, *Chem. Mater.* **1997**, *9*, 879.
[28] S. J. Sandoval, D. Yang, R. F. Frindt, J. C. Irwin, *Phys. Rev. B: Condens. Matter* **1991**, *44*, 3955.
[29] S. Gupta, E. Heintzman, J. Jasinski, *J. Raman Spectrosc.* **2015**, *46*, 217.
[30] D. Yang, S. J. Sandoval, W. M. R. Divigalpitiya, J. C. Irwin, R. F. Frindt, *Phys. Rev. B* **1991**, *43*, 12053.
[31] A. Berkdemir, H. R. Gutiérrez, A. R. Botello-Méndez, N. Perea-López, A. L. Elías, C. Chia, B. Wang, V. H. Crespi, F. López-Urías, J. C. Charlier, H. Terrones, M. Terrones, *Sci. Rep.* **2013**, *3*, 1755.
[32] L. Sun, J. Yan, D. Zhan, L. Liu, H. Hu, H. Li, B. K. Tay, J. L. Kuo, C. C. Huang, D. W. Hewak, P. S. Lee, Z. X. Shen, *Phys. Rev. Lett.* **2013**, *111*, 126801.
[33] S. S. Chou, N. Sai, P. Lu, E. N. Coker, S. Liu, K. Artyushkova, T. S. Luk, B. Kaehr, J. C. Brinker, *Nat. Commun.* **2015**, *6*, 8311.
[34] K. F. Mak, K. He, C. Lee, G. H. Lee, J. Hone, T. F. Heinz, J. Shan, *Nat. Mater.* **2013**, *12*, 207.
[35] Z. Ye, T. Cao, K. O'Brien, H. Zhu, X. Yin, Y. Wang, S. G. Louie, X. Zhang, *Nature* **2014**, *513*, 214.
[36] H. Qiu, T. Xu, Z. Wang, W. Ren, H. Nan, Z. Ni, Q. Chen, S. Yuan, F. Miao, F. Song, G. Long, Y. Shi, L. Sun, J. Wang, X. Wang, *Nat. Commun.* **2013**, *4*, 2642.
[37] J.-Y. Wang, G.-Y. Huang, S. Huang, J. Xue, D. Pan, J. Zhao, H. Xu, *Nano Lett.* **2018**, *8*, 4741.
[38] S. Bhattacharyya, A. K. Singh, *Phys. Rev. B* **2012**, *86*, 075454.
[39] S. N. Shirodkar, U. V. Waghmare, *Phys. Rev. Lett.* **2014**, *112*, 157601.
[40] W. Tang, E. Sanville, G. Henkelman, *J. Phys.: Condens. Matter* **2009**, *21*, 084204.
[41] E. Sanville, S. D. Kenny, R. Smith, G. Henkelman, *J. Comput. Chem.* **2007**, *28*, 899.
[42] G. Henkelman, A. Arnaldsson, H. Jónsson, *Comput. Mater. Sci.* **2006**, *36*, 354.

[43] S. Yan, W. Qiao, X. He, X. Guo, L. Xi, W. Zhong, Y. Du, *Appl. Phys. Lett.* **2015**, *106*, 012408.
[44] C. Ataca, S. Ciraci, *J. Phys. Chem. C* **2011**, *115*, 13303.
[45] L. Cai, J. He, Q. Liu, T. Yao, L. Chen, W. Yan, F. Hu, Y. Jiang, Y. Zhao, T. Hu, Z. Sun, S. Wei, *J. Am. Chem. Soc.* **2015**, *137*, 2622.
[46] H. Zheng, B. Yang, D. Wang, R. Han, X. Du, Y. Yan, *Appl. Phys. Lett.* **2014**, *104*, 132403.
[47] L. Wang, X. Liu, J. Luo, X. Duan, J. Crittenden, C. Liu, S. Zhang, Y. Pei, Y. Zeng, X. Duan, *Angew. Chem.* **2017**, *129*, 7718.
[48] K. Sangku, K. Jae-Hyeon, J. Ki-Joon, K. Yong-Hyun, Y. P. Jeong, *Nano Lett.* **2012**, *12*, 6043.
[49] Q. Li, X. Liu, S. Kim, V. B. Shenoy, P. E. Sheehan, J. T. Robinson, R. W. Carpick, *Nano Lett.* **2014**, *14*, 5212.
[50] J. S. Zabinski, J. E. Florkey, S. D. Walck, J. E. Bultman, N. T. McDevitt, *Surf. Coat. Technol.* **1995**, *76–77*, 400.
[51] P. Thomas, P. Bilas, A Molza, L. Legras, J. L. Mansot, K. Guerin, M. Dubois, in *New Fluorinated Carbons: Fundamentals and Applications*, Progress in Fluorine Science Series (Eds.: O. V. Boltalina, T. Nakajima), Elsevier Inc., **2017**, Ch. 14, pp. 325–360.
[52] R. L. Vander Wal, K. Miyoshi, K. W. Street, A. J. Tomasek, H. Peng, Y. Liu, J. L. Margrave, V. N. Khabashesku, *Wear* **2005**, *259*, 738.
[53] J. Ko, S. Kwon, I. Byun, J. Choi, B. Park, Y. Kim, J. Park, *Tribol. Lett.* **2013**, *50*, 137.
[54] D. B. Asay, S. H. Kim, *J. Phys. Chem. B* **2005**, *109*, 16760.

